JACS
JOURNAL OF THE AMERICAN CHEMICAL SOCIETY
pubs.acs.org/JACS
Article

Solar Fuel Synthesis Using a Semiartificial Colloidal Z-Scheme

Yongpeng Liu,[‖] Ariffin Bin Mohamad Annuar,[‖] Santiago Rodríguez-Jiménez, Celine Wing See Yeung, Qian Wang, Ana M. Coito, Rita R. Manuel, Inês A. C. Pereira, and Erwin Reisner*

Cite This: J. Am. Chem. Soc. 2024, 146, 29865−29876

Read Online

ACCESS | Metrics & More | Article Recommendations | Supporting Information

ABSTRACT: The integration of enzymes with semiconductor light absorbers in semiartificial photosynthetic assemblies offers an emerging strategy for solar fuel production. However, such colloidal biohybrid systems rely currently on sacrificial reagents, and semiconductor−enzyme powder systems that couple fuel production to water oxidation are therefore needed to mimic an overall photosynthetic reaction. Here, we present a Z-scheme colloidal enzyme system that produces fuel with electrons sourced from water. This "closed-cycle" semiartificial approach utilizes particulate $SrTiO_3$:La,Rh and $BiVO_4$:Mo (light absorbers), hydrogenase or formate dehydrogenase (cocatalyst), and a molecular cobalt complex (a redox mediator). Under simulated solar irradiation, this system continuously generates molecular hydrogen or formate, while co-producing molecular oxygen for 10 h using only sunlight, water, and carbon dioxide as inputs. In-depth analysis using quartz crystal microbalance, photoelectrochemical impedance spectroscopy, transient photocurrent spectroscopy, and intensity-modulated photovoltage spectroscopy provides mechanistic understanding and characterization of the semiconductor−enzyme hybrid interface. This study provides a rational platform to assemble functional semiartificial colloidal Z-scheme systems for solar fuel synthesis.

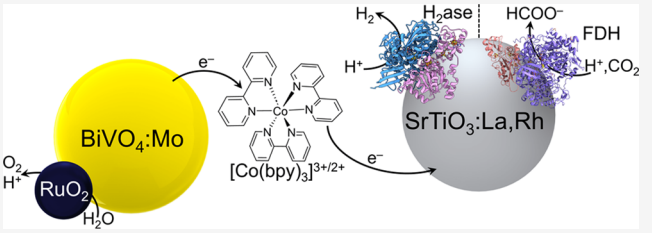

INTRODUCTION

Storing solar energy as chemical fuels and feedstocks provides a means to advance sustainable technologies.[1] Among emerging solar energy conversion approaches—photovoltaic-electrolysis, photoelectrochemistry, and photochemistry—the latter stands out due to its cost-effectiveness, device simplicity, and scalability.[2] Solar-powered hydrogen (H_2) production from water and carbon dioxide (CO_2) reduction coupled to water oxidation to oxygen (O_2) are particularly attractive solar fuel reactions (known as artificial photosynthesis).[3] These processes usually employ semiconductors as light absorbers along with cocatalysts for specific chemical half-reactions. However, achieving an efficient overall reaction on a single light absorber faces challenges, notably in balancing solar light absorption (requiring a narrow band gap) and producing high-energy photogenerated charges (requiring a large band gap).[4]

To address this issue, a photosynthesis-inspired Z-scheme system utilizes two light absorbers—a semiconductor to drive the reductive chemistry and a semiconductor for the oxidation reaction.[5] This artificial Z-scheme concept has been significantly advanced since its early development,[6] but some key challenges such as finding efficient light absorbers, facilitating charge mediation between the two semiconductors, and developing selective cocatalysts persist, hindering progress for this technology.

Various semiconductors, including oxides,[7] sulfides,[8] and nitrides,[9] have been explored as potential light absorbers in Z-scheme systems. $SrTiO_3$ stands out as a model semiconductor for photochemical systems due to its high-energy conduction band edge, favorable for driving both proton and CO_2 reduction.[10] However, its wide band gap limits its light absorption to the ultraviolet (UV) region, and extensive efforts have thus focused on doping $SrTiO_3$ with various elements to fine-tune its optoelectronic properties. For instance, Rh dopants can substitute Ti ions, creating intraband gap states that enable visible light absorption.[11] Co-doping with La atoms for Sr sites further controls the valence states, leading to the state-of-the-art $SrTiO_3$:La,Rh semiconductors for photoreductions.[9,12,13] Among oxidative semiconductors, $BiVO_4$ offers distinct advantages over TiO_2 and WO_3 for O_2 evolution due to its intrinsic catalytic activity, narrower band gap suitable for visible light absorption, and low-energy conduction band edge that prevents competing reduction reactions in a Z-scheme configuration.[14,15] Doping $BiVO_4$ with elements such as Mo and W increases charge separation efficiency, thereby enhancing its photocatalytic activity.[16]

Establishing efficient electron transfer between the two semiconductors presents an enormous challenge for constructing a functional Z-scheme system. Natural photosynthesis employs a Z-scheme with the cytochrome b_6f complex to shuttle electrons between photosystem I and photosystem II,

Received: August 27, 2024
Revised: September 30, 2024
Accepted: October 1, 2024
Published: October 16, 2024

https://doi.org/10.1021/jacs.4c11827
J. Am. Chem. Soc. 2024, 146, 29865−29876

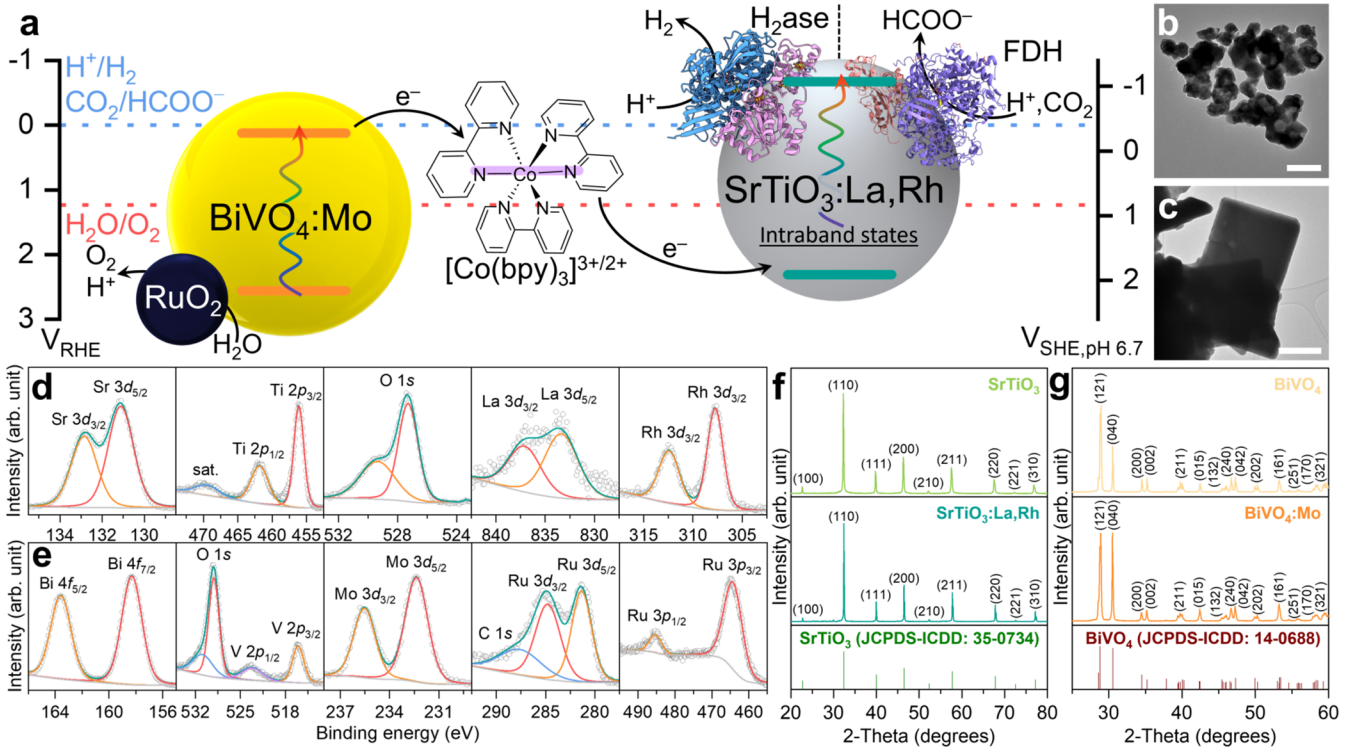

Figure 1. (a) Schematic illustration of a semiartificial colloidal Z-scheme system with H_2ase (PDB: 5jsh) and FDH (PDB: 6sdv). Estimated band positions for $SrTiO_3$:La,Rh and $BiVO_4$:Mo are given with redox potentials for $[Co(bpy)_3]^{3+/2+}$, H^+/H_2, $CO_2/HCOO^-$, and H_2O/O_2. TEM images of (b) $SrTiO_3$:La,Rh and (c) $BiVO_4$:Mo|RuO_2, scale bar: 500 nm. Curve-fitted XPS spectra of (d) $SrTiO_3$:La,Rh and (e) $BiVO_4$:Mo|RuO_2. Powder XRD patterns for (f) $SrTiO_3$ and $SrTiO_3$:La,Rh with the corresponding diffraction patterns for $SrTiO_3$ (JCPDS-ICDD: 35−0734) and (g) $BiVO_4$ and $BiVO_4$:Mo with the corresponding diffraction patterns for $BiVO_4$ (JCPDS-ICDD: 14−0688).

enabling the overall oxidation of water to O_2 and the fixation of CO_2 to carbohydrates.[17] In artificial Z-scheme systems, electron shuttles are categorized into soluble electron mediators (such as IO_3^-/I^-, $Fe^{3+/2+}$, and $Co^{3+/2+}$)[7,14,18] and solid-state mediators (including Au, graphene, and metal oxides).[8,13,19] Among soluble electron mediators, IO_3^-/I^- is more effective in alkaline conditions with pH greater than 9, and $Fe^{3+/2+}$ is only stable in acidic conditions with pH below 2.5. Molecular $Co^{3+/2+}$ complexes exhibit functionality across a wide pH range, with optimal activity observed at neutral pH. Notably, molecular $Co^{3+/2+}$ complexes have already demonstrated exceptional performance as redox couples for dye-sensitized solar cells, surpassing traditional I^-/I^{3-} redox shuttles and achieving power conversion efficiencies exceeding 13%.[20,21]

In a Z-scheme system aimed at catalyzing H_2 evolution and CO_2 reduction reactions, loading cocatalysts onto reductive semiconductors is essential for enabling efficient and selective solar fuel synthesis. Various synthetic catalysts, including Pt,[8] Ru,[14] Au,[22] and molecular 3d transition complexes,[12] have been extensively studied. However, achieving selective CO_2 conversion, especially toward products in the liquid phase, remains a significant challenge in this field.[5] In contrast to synthetic catalysts, nature has evolved dedicated enzymes to catalyze specific physiological processes. For instance, hydrogenases (H_2ases) and formate dehydrogenases (FDHs) facilitate the respective interconversion between proton and H_2, CO_2 and formate at the thermodynamic potential under mild conditions.[23,24] The integration of enzymes and light absorbers in a semiartificial approach has emerged as a promising research direction to leverage the performance strength of enzymes. However, a key challenge that persists is the reliance on sacrificial reagents for the functionality of colloidal semiartificial systems.[25,26] By mediating electron transfer between two semiconductors, a Z-scheme configuration can effectively preserve high-energy electrons and holes for specific reactions. This capability holds significant potential for achieving overall reactions without the need for sacrificial reagents in semiartificial photosynthesis. The application of enzymes as cocatalysts for selective solar fuel synthesis has been reported in photoelectrochemical tandem cells,[27,28] but interfacing enzymes with colloidal Z-scheme systems to couple water oxidation to fuel production remains a challenge.

In this study, we present a semiartificial colloidal photosynthetic Z-scheme system for solar fuel synthesis by coupling water oxidation to H_2 production or CO_2 reduction. The assembly of H_2ase or FDH enzymes with $SrTiO_3$:La,Rh|$[Co(bpy)_3]^{3+/2+}$|$BiVO_4$:Mo|RuO_2 (bpy = 2,2′-bipyridine) enables overall water splitting or CO_2 reduction to formate coupled to O_2 evolution, respectively. A benefit of using a semiconductor suspension system is their operation in bulk (3D) solution without the complex device construction process and confined two-dimensional (2D) surface in photoelectrodes,[27,28] artificial leaves,[29] and photocatalyst sheets.[12,13] The semiconductor light absorbers were characterized by Mott−Schottky analysis to confirm the suitable band edge positions of $SrTiO_3$:La,Rh and $BiVO_4$:Mo. The adsorption of enzymes onto the reductive semiconductor was studied by using a quartz crystal microbalance (QCM). Furthermore, we investigated the charge carrier dynamics of the semiartificial Z-scheme systems using photoelectrochemical techniques such as photoelectrochemical impedance

https://doi.org/10.1021/jacs.4c11827
J. Am. Chem. Soc. 2024, 146, 29865−29876

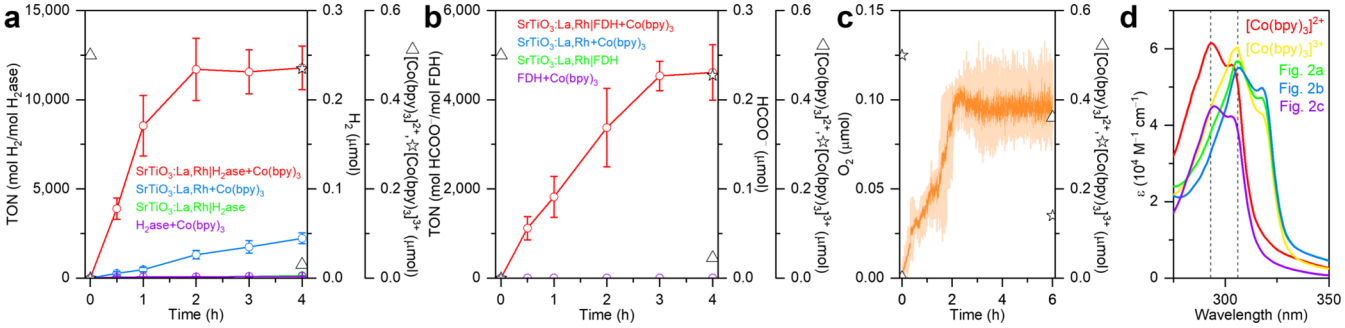

Figure 2. Z-scheme half reactions with $SrTiO_3$:La,Rh coupled to stoichiometric $[Co(bpy)_3]^{2+}$ oxidation using (a) H_2ase for photocatalytic proton reduction to H_2 and (b) FDH for photocatalytic reduction of CO_2 to formate. (c) Z-scheme half reaction with $BiVO_4$:Mo|RuO_2 coupled to stoichiometric $[Co(bpy)_3]^{3+}$ reduction for photocatalytic water oxidation to O_2. (d) UV absorption spectra of aqueous standard $[Co(bpy)_3]^{3+/2+}$ solutions and post photocatalysis solutions. Conditions: a CO_2-saturated aqueous solution (1 mL, pH 6.7) containing $NaHCO_3$ (0.1 M), $[Co(bpy)_3]^{3+/2+}$ (0.5 μmol), $SrTiO_3$:La,Rh (1 mg), $BiVO_4$:Mo|RuO_2 (1 mg), H_2ase (20 pmol), FDH (50 pmol), AM 1.5G irradiation, 600 rpm stirring, 25 °C. Error bars represent the standard deviation for a sample size of 3.

spectroscopy (PEIS), intensity-modulated photovoltage spectroscopy (IMVS), and transient photocurrent spectroscopy (TPC).

RESULTS AND DISCUSSION

Selection and Characterizations. [NiFeSe]-H_2ase and [W]-FDH from *Desulfovibrio vulgaris* Hildenborough (*Dv*H) were chosen as model enzymes due to their selective and reversible catalysis (very low overpotential requirement) for H_2 evolution and CO_2-to-formate conversion under mild conditions, respectively. Furthermore, the enzymes attach strongly to metal oxides in an electroactive configuration, and display a moderate tolerance to O_2.[23,24,30] For the fuel-forming (reduction) semiconductor, $SrTiO_3$:La,Rh was selected due to its high conduction band edge, excellent dispersity in solution, and visible light absorption properties.[11,31] RuO_2 was loaded as the cocatalyst onto the oxidation semiconductor $BiVO_4$:Mo, specifically designed for water oxidation.[12,13]

Figure 1a depicts the proposed semiartificial colloidal photosynthetic Z-scheme for solar H_2 production or solar CO_2-to-formate conversion using water as the electron donor. Tauc plots (Figure S1) and Mott−Schottky analysis (Figure S2) confirmed the band diagram of $SrTiO_3$:La,Rh and $BiVO_4$:Mo, where both the conduction band edge (E_C) and the valence band edge (E_V) of $SrTiO_3$:La,Rh are higher than those of $BiVO_4$:Mo, and the band gaps of the two semiconductors overlap,[9,12,13] illustrating a suitable energy band alignment between the two semiconductors for constructing a Z-scheme system. Cyclic voltammetry analysis of the $[Co(bpy)_3]^{3+/2+}$ complex revealed a half-wave potential ($E_{1/2}$) of 0.70 V *vs* the reversible hydrogen electrode (RHE).[14] This value falls within the band gaps of both $SrTiO_3$:La,Rh and $BiVO_4$:Mo, showing the suitability of $[Co(bpy)_3]^{3+/2+}$ as an electron mediator for the proposed Z-scheme system, and is in agreement with the literature.[9,12,14]

Upon irradiation, photogenerated holes in the valence band of $BiVO_4$:Mo transfer to RuO_2 for the oxygen evolution reaction (OER), while photogenerated electrons in the conduction band reduce $[Co(bpy)_3]^{3+}$ to $[Co(bpy)_3]^{2+}$. Meanwhile, photogenerated holes in the intraband states of $SrTiO_3$:La,Rh oxidize $[Co(bpy)_3]^{2+}$ back to $[Co(bpy)_3]^{3+}$, while the photogenerated electrons in the conduction band either reduce protons to H_2 (when paired with H_2ase) or reduce CO_2 to formate (when paired with FDH). The regeneration of the $[Co(bpy)_3]^{3+/2+}$ redox couple allows the spatial separation of photogenerated electrons and holes in the two semiconductors, thereby enhancing charge separation efficiency and preserving high-energy photogenerated charges for catalyzing the corresponding reactions.

Scanning electron microscopy (SEM) and transmission electron microscopy (TEM) revealed the morphology of $SrTiO_3$:La, Rh nanoparticles and RuO_2 loaded $BiVO_4$:Mo nanoplates (Figures 1b−c and S3−S8). The presence of individual elements of $SrTiO_3$:La,Rh and $BiVO_4$:Mo was confirmed through energy-dispersive X-ray (EDX) mapping (Figures S9−S11) and X-ray photoelectron spectroscopy (XPS, Figure 1d−e). To identify lattice changes induced by doping, powder X-ray diffraction (XRD) analysis was conducted on both pristine and doped metal oxide semiconductors. The XRD pattern of $SrTiO_3$:La,Rh, compared to pristine $SrTiO_3$, retains the cubic structure (Figure 1f) but exhibits a peak shift toward higher angles (Figure S12a). This shift indicates a successful doping process, reflecting changes in lattice parameters due to the substitution of Sr^{2+} (0.144 nm) and Ti^{4+} (0.060 nm) ions with La^{3+} (0.136 nm) and Rh^{3+} (0.068 nm) ions.[32] Additionally, the XRD pattern of $BiVO_4$:Mo corresponds to the monoclinic phase of $BiVO_4$, with no evidence of secondary phases such as MoO_x (Figure 1g). The observed peak shift confirms the successful substitution of Mo^{6+} ions (0.059 nm) with V^{5+} ions (0.054 nm) within the $BiVO_4$ crystal lattice (Figure S12b).[33] These peak shifts are expected, as doping alters the *d*-spacing due to differences in the ionic radii of the dopant and host atoms. The absorption profiles of $SrTiO_3$:La,Rh and $BiVO_4$:Mo were characterized by ultraviolet−visible (UV−vis) spectroscopy (Figure S13).

With the aim of maintaining the *in vitro* activity of H_2ases and FDHs under benign conditions, the $[Co(bpy)_3]^{3+/2+}$ redox mediator was identified as an ideal candidate due to its outstanding activity at neutral pH. Water-soluble $[Co(bpy)_3]$-SO_4 was synthesized following a reported procedure[14,34] (reaction scheme and photograph in Figures S14 and S15) and characterized using elemental analysis, mass spectrometry, proton nuclear magnetic resonance (^{1}H NMR) spectroscopy (Experimental Section, Figure S16), attenuated total reflectance Fourier-transform infrared (ATR-FTIR) spectroscopy (Figure S17), and UV−vis spectroscopy (Figure S18).

Photocatalytic Half Reactions. We started the stepwise construction of a functional Z-scheme system by conducting Z-

https://doi.org/10.1021/jacs.4c11827
J. Am. Chem. Soc. 2024, 146, 29865−29876

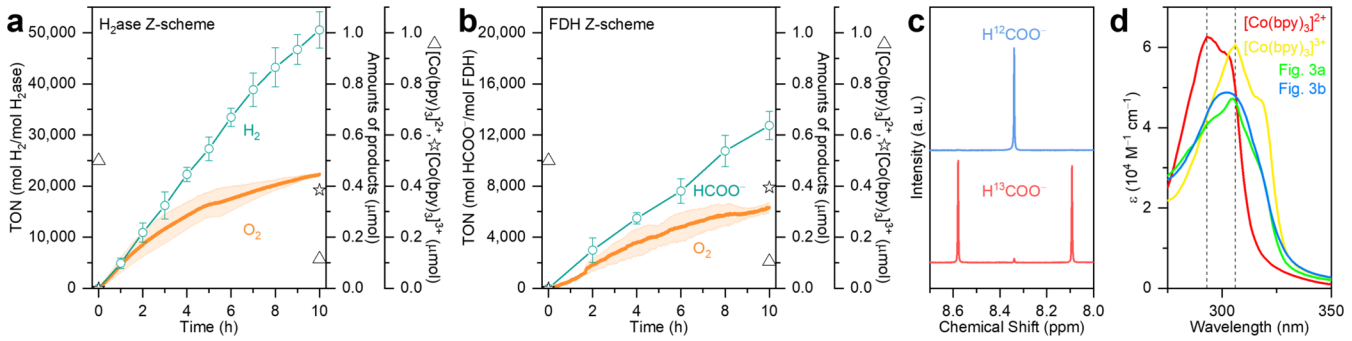

Figure 3. (a) Photocatalytic overall water splitting using the Z-scheme H_2ase|$SrTiO_3$:La,Rh|$[Co(bpy)_3]^{3+/2+}$|$BiVO_4$:Mo|RuO_2. (b) Photocatalytic reduction of CO_2 to formate coupled with water oxidation using the Z-scheme FDH|$SrTiO_3$:La,Rh|$[Co(bpy)_3]^{3+/2+}$|$BiVO_4$:Mo|RuO_2. (c) ^{1}H NMR spectra of the photocatalysis solution containing $^{12}CO_2$/$NaH^{12}CO_3$ (blue line) and $^{13}CO_2$/$NaH^{13}CO_3$ (red line) after 10 h of irradiation on FDH|$SrTiO_3$:La,Rh|$[Co(bpy)_3]^{3+/2+}$|$BiVO_4$:Mo|RuO_2. (d) UV absorption spectra of aqueous standard $[Co(bpy)_3]^{3+/2+}$ solutions and post photocatalysis solutions. Conditions: a CO_2-saturated aqueous solution (1 mL, pH 6.7) containing $NaHCO_3$ (0.1 M), $[Co(bpy)_3]SO_4$ (0.5 μmol), $SrTiO_3$:La,Rh (1 mg), $BiVO_4$:Mo|RuO_2 (1 mg), H_2ase (20 pmol), FDH (50 pmol), AM 1.5G irradiation, 600 rpm stirring, 25 °C. Error bars represent the standard deviation for a sample size of 3.

scheme half reactions separately on the reduction and oxidation semiconductors, respectively, with the counter-reaction balanced by the stoichiometric conversion of the $[Co(bpy)_3]^{3+/2+}$ redox mediator. In a colloidal system, photocatalytic H_2 production was established by interfacing H_2ase (20 pmol) with $SrTiO_3$:La,Rh (1 mg) in a CO_2-saturated aqueous solution (1 mL) containing $NaHCO_3$ (0.1 M) and $[Co(bpy)_3]SO_4$ (0.5 μmol) under simulated AM 1.5G irradiation at 25 °C. The solutions with H_2ase contained CO_2-saturated $NaHCO_3$ to match the anaerobic conditions using FDH (see below).

The time dependent H_2 evolution (Figure 2a and Table S1) displayed a linear increase in the first hour, saturating after 2 h at 0.234 ± 0.035 μmol H_2, corresponding to a turnover number (TON) of 11,700. The TON is determined by the ratio of moles product (H_2) to moles enzyme (H_2ase).[35] The *in vitro* activity of H_2ase ceased after 2 h because of the stoichiometric consumption of $[Co(bpy)_3]SO_4$. Considering that H_2 evolution is a two-electron transfer process, the saturated H_2 yield corresponds to 0.468 μmol of consumed electrons and closely matches the 0.5 μmol of $[Co(bpy)_3]^{2+}$ in the solution. This confirms that $SrTiO_3$:La,Rh|H_2ase assemblies can simultaneously reduce protons to H_2 and oxidize $[Co(bpy)_3]^{2+}$ to $[Co(bpy)_3]^{3+}$, establishing the foundation for the reduction half reaction of a Z-scheme system. The depletion of $[Co(bpy)_3]^{2+}$ in the solution was confirmed by UV−vis spectroscopy (Figure 2d) using the quantification method based on the Beer−Lambert law: $A = \varepsilon cl$, where A is the absorbance, ε is the molar absorption coefficient (M^{-1} cm^{-1}), c is the molar concentration (M), and l is the optical path length (cm) (see Experimental Section).[14,36] This method is based on the principle that changes in the $Co(bpy)_3$ valence state affect the $\pi-\pi^*$ transitions of ligands, leading to alterations in UV absorption. An increase in the central Co ion valence from 2+ to 3+ results in a bathochromic shift (red shift) in the absorption spectrum from 293 to 306 nm.[36−38] The ε of $[Co(bpy)_3]SO_4$ was found to be 6.209 × 10^4 M^{-1} cm^{-1}, similar to the previous reports for $[Co(bpy)_3]SO_4$ (6.958 × 10^4 M^{-1} cm^{-1})[14] and $[Co(bpy)_3](ClO_4)_2$ (4.2 × 10^4 M^{-1} cm^{-1}).[36] After 4 h of photocatalysis, 0.47 μmol of $[Co(bpy)_3]^{3+}$ was produced, corresponding to a 94% conversion yield for Co^{2+} to Co^{3+}. Kudo and co-workers previously identified Rh ions in $SrTiO_3$:Rh as the active sites for $[Co(bpy)_3]^{2+}$ oxidation.[14]

Exclusion control experiments (Figure 2a and Table S1) were conducted by systematically removing individual components from the photocatalytic system. As depicted in Figure 2a, no photocatalytic H_2 generation was observed in the absence of $SrTiO_3$:La,Rh_4. The absence of $[Co(bpy)_3]$ resulted in no H_2 production, indicating that $[Co(bpy)_3]^{2+}$ is the exclusive electron donor in the system, and $SrTiO_3$:La,Rh alone cannot catalyze overall water splitting. In the absence of H_2ase, $SrTiO_3$:La,Rh produced a minor amount of H_2, reaching a yield of 0.04 ± 0.006 μmol of H_2 over 4 h. This observation suggests that dopants in $SrTiO_3$:La,Rh such as Rh sites can catalyze some H_2 production.[39]

The reduction half reaction on $SrTiO_3$:La,Rh|FDH assemblies in a CO_2-saturated aqueous solution (1 mL) containing $NaHCO_3$ (0.1 M), $[Co(bpy)_3]SO_4$ (0.5 μmol), $SrTiO_3$:La,Rh (1 mg), and FDH (50 pmol) under simulated AM 1.5G irradiation resulted in a linear solar formate production that saturated at 4 h with 0.230 ± 0.031 μmol, corresponding to a TON_{FDH} of 4,614 (Figure 2b and Table S2). The two-electron transfer CO_2-to-formate reaction consumed 0.454 μmol of photogenerated electrons, consistent with the initial 0.5 μmol of $[Co(bpy)_3]^{2+}$ in the solution and the 0.455 μmol of $[Co(bpy)_3]^{3+}$ measured after 4 h of photocatalysis (Figure 2d, Co^{2+} to Co^{3+} conversion yield: 91%). Notably, this solar formate production half reaction could not be achieved in the absence of any components (Figure 2b and Table S2), indicating that FDH is the sole catalyst in the system capable of reducing CO_2. This study also demonstrates direct electron transfer between a $SrTiO_3$-based semiconductor and enzymes, providing further support for the notion that metal oxides serve as excellent scaffolds for accommodating enzymes in their active orientations.[27−30]

The oxidation half reactions were conducted on $BiVO_4$:Mo|RuO_2 (1 mg) with $[Co(bpy)_3]_2(SO_4)_3$ (0.5 μmol) in a CO_2-saturated aqueous solution (1 mL) containing $NaHCO_3$ (0.1 M) under simulated AM 1.5G irradiation at 25 °C. As shown in Figure 2c, a linear increase in O_2 production over 2.2 h is followed by saturation at around 0.1 μmol. Considering the four-electron water oxidation, approximately 0.4 μmol of photogenerated holes were consumed, indicating that the termination of O_2 production was due to the depletion of

https://doi.org/10.1021/jacs.4c11827
J. Am. Chem. Soc. 2024, 146, 29865−29876

$[Co(bpy)_3]^{3+}$. The conversion yield of Co^{3+} to Co^{2+} was found to be 72% (Figure 2d). By completing all three half reactions, we have confirmed the suitability of the $SrTiO_3$:La,Rh|enzyme biohybrids for the reduction half reaction and $BiVO_4$:Mo|RuO_2 for the oxidation half reaction, thereby establishing the foundation for constructing a functional semiartificial Z-scheme system using $[Co(bpy)_3]^{3+/2+}$ as the redox mediator.

Photosynthetic Z-Scheme Systems. A semiartificial Z-scheme system for overall water splitting was subsequently developed using a colloidal suspension consisting of $SrTiO_3$:La,Rh|H_2ase powder and $BiVO_4$:Mo|RuO_2 powder dispersed in an aqueous solution containing $[Co(bpy)_3]SO_4$ (0.5 μmol), giving H_2ase|$SrTiO_3$:La,Rh|$[Co(bpy)_3]^{3+/2+}$|$BiVO_4$:Mo|RuO_2, in a CO_2-saturated $NaHCO_3$ (0.1 M) solution (1 mL, pH 6.7) under simulated AM 1.5G irradiation at 25 °C (Figure 3a and Table S3). Unlike the early termination observed in individual half reactions (Figure 2), the full Z-scheme system demonstrated the ability to generate solar H_2 continuously over a period of 10 h in a nearly linear manner, accompanied by simultaneous solar O_2 production.

This outcome supports our hypothesis (Figure 1a) that the $[Co(bpy)_3]^{3+/2+}$ redox couple, acting as the electron shuttle, is cycled by the photogenerated holes in $SrTiO_3$:La,Rh and by the photogenerated electrons in $BiVO_4$:Mo. The colloidal photosynthetic Z-scheme system achieved a H_2 production yield of 1.01 ± 0.07 μmol (corresponds to an activity, based on the mass of the photocatalyst, of 50.6 ± 3.6 μmol g^{-1} h^{-1}) and O_2 production of 0.45 ± 0.004 μmol (corresponds to an activity of 22.4 ± 0.2 μmol g^{-1} h^{-1}) in 10 h. The turnover frequency (TOF) for H_2 reached 5,055 h^{-1} in 10 h (Table S4). The apparent quantum yield (AQY) at 420 nm and the solar-to-H_2 energy conversion efficiency (STH) were found to be 0.8% and 0.007% (10 h), respectively. The molar ratio between H_2 and O_2 was nearly stoichiometric at approximately 2:0.89 at 10 h.[5,14] In overall water splitting, separate gas evolution is particularly crucial for large-scale H_2 production due to the formation of explosive H_2 and O_2 gas mixtures as well as requiring O_2-free H_2 for downstream use of H_2 (*e.g.*, hydrogenation chemistry, use in fuel cells).[40] However, this aspect is beyond the scope of our present research, which primarily focuses on demonstrating fundamental research in constructing colloidal biohybrids for photocatalysis and producing H_2 on a μmol scale.

After 10 h of photocatalysis, the ratio of $[Co(bpy)_3]^{2+}$ to $[Co(bpy)_3]^{3+}$ was approximately 1 to 3.3 (Figure 3a,d), indicating the predominance of trivalent $[Co(bpy)_3]$ post photocatalysis. The turnover frequency for cycling $[Co(bpy)_3]^{3+/2+}$ in the overall water splitting is 0.52 h^{-1}. Similar observations were reported by Kudo and colleagues, who noted a 1 to 9 ratio for $[Co(phen)_3]^{2+}$ to $[Co(phen)_3]^{3+}$ after long-term photocatalysis using $[Co(phen)_3]^{3+/2+}$ as the redox mediator for Z-scheme reactions.[14] The authors also reported that the TOF of $[Co(bpy)_3]^{3+/2+}$ electron mediator with $SrTiO_3$:Rh|Ru is 0.32 h^{-1} (without Sr excess) and 3.3 h^{-1} (with Sr excess).[14]

Semiartificial solar CO_2-to-formate production coupled with O_2 evolution was performed using the FDH|$SrTiO_3$:La,Rh|$[Co(bpy)_3]^{3+/2+}$|$BiVO_4$:Mo|RuO_2 suspension in a CO_2-saturated aqueous solution (1 mL) containing $NaHCO_3$ (0.1 M) and $[Co(bpy)_3]SO_4$ (0.5 μmol) under simulated AM 1.5G irradiation at 25 °C (Figure 3b and Table S3). The overall reaction was sustained for 10 h, resulting in the production of 0.64 ± 0.05 μmol (31.9 ± 2.7 μmol g^{-1} h^{-1}) of formate and 0.32 ± 0.02 μmol (15.8 ± 1.0 μmol g^{-1} h^{-1}) of O_2. The TOF of formate over 10 h was 1274 h^{-1} (Table S4). The lower TOF values compared to H_2 production is attributed to FDH having a slower specific activity than H_2ase. The ratio of $[Co(bpy)_3]^{2+}$ to $[Co(bpy)_3]^{3+}$ was found to be around 1 to 3.8 after 10 h of photocatalysis (Figure 3b,d) with a TOF for $[Co(bpy)_3]^{3+/2+}$ of 0.33 h^{-1}. The AQY at 420 nm and the solar-to-formate energy conversion efficiency (STF) were found to be 0.5% and 0.004% (10 h), respectively.

In addition to utilizing the full simulated solar spectrum, additional experiments were conducted under UV-free visible light irradiation (λ > 420 nm). The Z-scheme H_2ase|$SrTiO_3$:La,Rh|$[Co(bpy)_3]^{3+/2+}$|$BiVO_4$:Mo|RuO_2 system produced 177 ± 9 nmol H_2 in 4 h when irradiated with light >420 nm, compared to 446 ± 28 nmol H_2 under AM 1.5G irradiation (Figure S19a). Similarly, the Z-scheme FDH|$SrTiO_3$:La,Rh|$[Co(bpy)_3]^{3+/2+}$|$BiVO_4$:Mo|RuO_2 system generated 120 ± 16 nmol formate at >420 nm and 274 ± 22 nmol formate under AM 1.5G conditions (Figure S19b).

To evaluate the scalability of the Z-scheme system, photocatalysis experiments were conducted in a larger photoreactor, scaled up by a factor of 6 (Figure S20). Using a 6 mL Z-scheme colloidal suspension, the system produced 1890 ± 201 nmol of H_2 and 1338 ± 189 nmol of formate in 4 h when coupled with H_2ase and FDH, respectively (Figure S21). These values are 4.2 and 4.9 times higher than those obtained with a 1 mL colloidal suspension. The mismatch in the scale-up factor between volumes and products is attributed to the challenges in maintaining turbulent mixing in a larger stirred photoreactor, leading to partially stationary solutions. For fast turnover cocatalysts, such as molecular catalysts and enzymes, stationary solutions can cause mass transport limitations and local pH changes, resulting in reduced product yields.

To unambiguously confirm the carbon source for solar formate production, isotopic labeling experiments were conducted. Z-scheme photocatalysis experiments were carried out using either an aqueous $NaH^{12}CO_3$ solution (0.1 M) with $^{12}CO_2$ as the headspace gas or an aqueous $NaH^{13}CO_3$ solution (0.1 M) with $^{13}CO_2$ as the headspace gas. ^{1}H NMR spectra were collected after 10 h of simulated AM 1.5G irradiation (Figure 3c), showing a singlet signal of $H^{12}COO^-$ (using $^{12}CO_2$ and $NaH^{12}CO_3$) and a doublet signal of $H^{13}COO^-$ (using $^{13}CO_2$ and $NaH^{13}CO_3$). ^{1}H NMR spectra of commercial sodium formate-^{12}C ($H^{12}COONa$) and sodium formate-^{13}C ($H^{13}COONa$) were recorded for comparison (Figure S22). These results confirm that formate originated from CO_2 reduction reactions, not from contaminations or side reactions. The Z-scheme $SrTiO_3$:La,Rh|$[Co(bpy)_3]^{3+/2+}$|$BiVO_4$:Mo|RuO_2 photocatalytic system containing either H_2ase or FDH as the biological components generated O_2 below 0.1% volume percent within the photoreactor, which falls within the oxygen tolerance range reported for both enzymes.[23,24]

Stability of the $[Co(bpy)_3]^{3+/2+}$ Redox Couple. To study the stability of the $[Co(bpy)_3]^{3+/2+}$ redox couple, a series of electrochemical experiments, including cyclic voltammetry (CV) and chronoamperometry (CA), were conducted. During the initial 10 h of CA (Figure 4a), $[Co(bpy)_3]^{2+}$ was oxidized to $[Co(bpy)_3]^{3+}$ at 0.9 V *vs* RHE, with the total charge passed reaching 2.23 μmol. Given that the electrochemistry was performed in a 5 mL of electrolyte containing 0.5 mM $[Co(bpy)_3]^{2+}$, the maximum available amount of $[Co(bpy)_3]^{2+}$

https://doi.org/10.1021/jacs.4c11827
J. Am. Chem. Soc. 2024, 146, 29865−29876

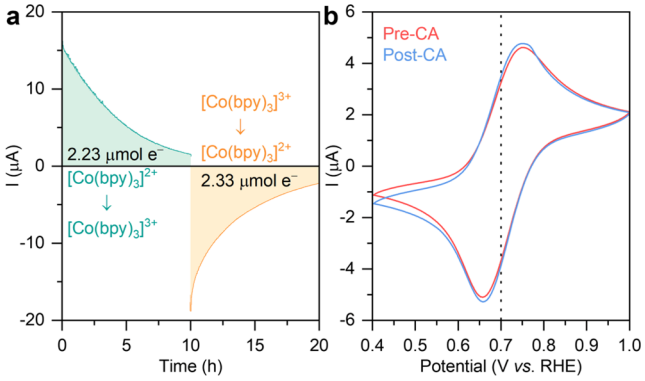

Figure 4. (a) Chronoamperometry of $[Co(bpy)_3]^{2+}$ oxidation at 0.9 V *vs* RHE and $[Co(bpy)_3]^{3+}$ reduction at 0.5 V *vs* RHE for 20 h. (b) Cyclic voltammetry (10 mV s^{-1}, third scan) of $[Co(bpy)_3]^{3+/2+}$ before and after CA. The dotted line represents the redox potential. Electrolyte: a CO_2-saturated solution (5 mL, pH 6.7) containing $NaHCO_3$ (0.1 M), $[Co(bpy)_3]^{2+}$ (0.5 mM), and KCl (50 mM). 3-electrode configuration: Toray carbon paper working electrode (0.25 cm^2), Ag/AgCl (saturated KCl) reference electrode, Pt mesh counter electrode.

is 2.5 μmol, indicating the near-complete depletion of $[Co(bpy)_3]^{2+}$ in solution. Subsequently, the reduction of $[Co(bpy)_3]^{3+}$ (from the oxidized sample above) to $[Co(bpy)_3]^{2+}$ was conducted for another 10 h at 0.5 V *vs* RHE with a total charge pass of 2.33 μmol, representing the depletion of $[Co(bpy)_3]^{3+}$. The redox ability of the $[Co(bpy)_3]^{3+/2+}$ mediator was evaluated by CV, showing no significant deformation in CV traces (Figure 4b), indicating stability for at least 20 h. This demonstrates the suitability of the $[Co(bpy)_3]^{3+/2+}$ redox mediator under conditions used for the photocatalysis study presented herein.

Characterization of Semiconductor-Enzyme Interface. The interactions between $SrTiO_3$:La,Rh and enzymes were investigated by using QCM analysis. A gold-coated quartz chip was functionalized with a thin layer of $SrTiO_3$:La,Rh by drop-casting an ultrasonicated suspension (0.1 mL) of $SrTiO_3$:La,Rh (0.5 mg mL^{-1}) in isopropanol, mimicking *operando* conditions during photocatalysis. As depicted in Figure 5, after establishing a stable baseline for 10 min, 50 pmol of enzymes (either H_2ase or FDH) were introduced into an aqueous solution (2 mL) containing $NaHCO_3$ (0.1 M) and $[Co(bpy)_3]SO_4$ (0.5 mM) under anaerobic conditions, with the solution flowing toward the QCM chip at a rate of 0.141 mL min^{-1}. The enzyme loading was monitored and quantified by converting the frequency change into mass change using the Sauerbrey equation.[41]

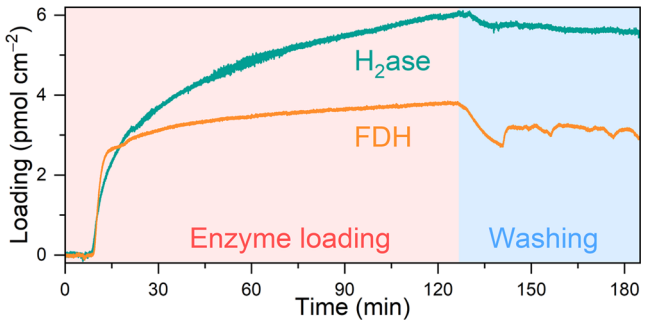

Figure 5. QCM analysis of the adsorption process and washing process of H_2ase and FDH on a $SrTiO_3$:La,Rh-coated quartz chip. Loading conditions: 0.141 mL min^{-1} flow rate, an anaerobic aqueous solution (2 mL, pH 6.7) containing $NaHCO_3$ (0.1 M), $[Co(bpy)_3]SO_4$ (0.5 mM), and 50 pmol of enzymes (either H_2ase or FDH), 25 °C. Washing conditions: 0.141 mL min^{-1} flow rate, an anaerobic aqueous solution (10 mL, pH 6.7) containing $NaHCO_3$ (0.1 M) and 0.5 mM $[Co(bpy)_3]^{3+/2+}$, 25 °C.

The adsorption of both enzymes on $SrTiO_3$:La,Rh exhibited two distinct stages: a rapid adsorption stage lasting until 22 min for H_2ase and 13 min for FDH, followed by a slower adsorption stage until reaching an enzyme loading of 6.0 pmol cm^{-2} for H_2ase and 3.8 pmol cm^{-2} for FDH after 2 h. Following enzyme loading, a washing process was conducted to assess the robustness of the enzyme binding with $SrTiO_3$:La,Rh. An enzyme-free aqueous solution (10 mL) containing $NaHCO_3$ (0.1 M) and $[Co(bpy)_3]SO_4$ (0.5 mM) was flowed at a rate of 0.141 mL min^{-1} for 1 h (Figure 5). It was observed that after enzymes were loaded onto the $SrTiO_3$:La,Rh surface, their binding was strong, with only 7% of H_2ase and 18% of FDH being desorbed after 1 h of washing.[30] QCM studies thus confirm the robust binding between enzymes and the $SrTiO_3$:La,Rh photocatalyst.

Mechanistic Insights into Charge Carrier Dynamics. To investigate the charge carrier dynamics between the enzymes and $SrTiO_3$:La,Rh, we conducted photoelectrochemical techniques, namely PEIS, TPC, and IMVS, on $SrTiO_3$:La,Rh photoelectrodes. The photoelectrodes were prepared by drop-casting a $SrTiO_3$:La,Rh suspension in isopropanol (50 μL of 2 mg mL^{-1}) onto a masked FTO-coated glass, resulting in an active area of 0.25 cm^2.[12]

PEIS measurements were performed on pristine $SrTiO_3$:La,Rh, $SrTiO_3$:La,Rh|H_2ase, and $SrTiO_3$:La,Rh|FDH under simulated AM 1.5G irradiation by applying a sinusoidal voltage modulation between the working electrode and the reference electrode in an electrochemical cell with a three-electrode configuration. The impedance response displayed a single semicircle for all three samples in Figure 6a, without signs of diffusional impedance (Warburg impedance).[42] Qualitatively, upon introducing enzymes (either H_2ase or FDH), the semicircle's diameter decreased, indicating a facilitated charge transfer process for Faradaic reactions.

Quantitative analysis was based on fitting the impedance response with a Randles equivalent circuit (Figure 6a inset)[43] comprising a series resistor (R_S) in series with a parallel combination of a bulk capacitor (C_{bulk}) and a charge transfer resistor (R_{ct}). R_S represents the sum of all non-Faradaic processes in the electrochemical system, including electrolyte resistance, contact resistance, and lead resistance. All three samples exhibited an R_S value around 188 Ω (Table S5). R_{ct} describes the Faradaic process of the system, specifically the difficulty of electron transfer at the electrode−electrolyte interface.[44] The assembly between H_2ase and $SrTiO_3$:La,Rh decreased R_{ct} from 15.7 ± 0.16 to 6.8 ± 0.09 kΩ, indicating the role of H_2ase as cocatalysts for catalyzing hydrogen evolution reaction (HER). Similarly, $SrTiO_3$:La,Rh|FDH showed a decreased R_{ct} of 8.7 ± 0.09 kΩ, indicating the role of FDH in facilitating CO_2 reduction to formate. The lower R_{ct} observed for $SrTiO_3$:La,Rh|H_2ase compared to $SrTiO_3$:La,Rh|FDH aligns well with the difference in product yields during photocatalysis. This can be attributed to the inherently slower specific activity of FDH for CO_2 reduction compared to H_2ase for HER. According to the fitting results, the pseudo first-order rate constant for charge transfer (k_{ct}) of the Faradaic process

https://doi.org/10.1021/jacs.4c11827
J. Am. Chem. Soc. 2024, 146, 29865−29876

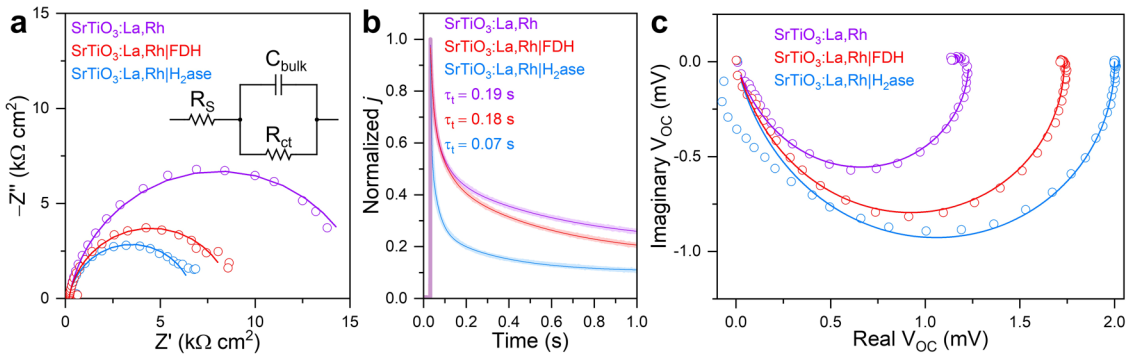

Figure 6. (a) Nyquist plots of the PEIS response recorded at −0.2 V *vs* RHE (open circuits) with corresponding fitted curves (solid lines). Inset: proposed equivalent circuit to fit the impedance response. (b) Normalized TPC response recorded at −0.2 V *vs* RHE with corresponding exponential fitted curves. (c) Nyquist plots of the IMVS response (open circuits) with corresponding phenomenological fitted curves (solid lines). Conditions: a CO_2-saturated aqueous solution (20 mL, pH 6.7) containing $NaHCO_3$ (0.1 M), $[Co(bpy)_3]SO_4$ (0.5 mM), and KCl (50 mM). $SrTiO_3$:La,Rh, working electrode; Ag/AgCl (sat. KCl), reference electrode; Pt mesh, counter electrode; AM 1.5G irradiation; and 25 °C.

was determined based on the phenomenological model developed for photoelectrodes under irradiation.[45] The values of k_{ct} for pristine $SrTiO_3$:La,Rh, $SrTiO_3$:La,Rh|H_2ase, and $SrTiO_3$:La,Rh|FDH were 2.6, 7.6, and 4.8 s^{-1}, respectively, further confirming that enzymes can facilitate the kinetics of charge transfer processes for dedicated reactions.

In addition to investigating the reduction half reaction, PEIS was performed on $BiVO_4$:Mo and $BiVO_4$:Mo|RuO_2 to study the oxidation half reaction, thereby complementing the full Z-scheme reactions (Figure S23). Randles equivalent circuit fitting reveals that the incorporation of RuO_2 on $BiVO_4$:Mo decreases the R_{ct} from 153.3 ± 19.44 to 79.1 ± 6.91 kΩ (Table S5). This reduction in R_{ct} supports the effectiveness of RuO_2 as an efficient OER cocatalyst in Z-scheme systems.

The impact of enzymes on the electron extraction process of $SrTiO_3$:La,Rh was evaluated using TPC, as depicted in Figure 6b. By employing exponential fitting on the normalized TPC response, we determined the electron transit time (τ_t) values for pristine $SrTiO_3$:La,Rh, $SrTiO_3$:La,Rh|H_2ase, and $SrTiO_3$:La,Rh|FDH. Our findings revealed that interfacing H_2ases with $SrTiO_3$:La,Rh significantly decreased τ_t from 0.19 to 0.07 s, indicating photogenerated electrons can be effectively collected by H_2ase for HER, thereby enhancing the electron transport process within $SrTiO_3$:La,Rh. A similar trend was observed for $SrTiO_3$:La,Rh|FDH, resulting in a slightly reduced τ_t value of 0.18 s.

Furthermore, IMVS was utilized to gain insights into charge recombination dynamics. This technique is well-established in solar cell research and has gained increased attention for evaluating electron lifetime in photoelectrochemical systems.[46,47] By sinusoidally modulating incident light intensity, IMVS recorded the complex-valued open circuit photovoltage response (V_{OC}). To accurately determine the first-order electron lifetime (τ_n) of the system, phenomenological fitting of the Nyquist plot was carried out (Figure 6c):[48,49]

$$V_{OC}(\omega) = \frac{V_{SS}}{(1 + i\omega\tau_n)^{\alpha}}$$

where, V_{SS} is steady-state photovoltage, ω is angular frequency, and α ($0 < \alpha \leq 1$) is introduced as a nonideality factor to account for surface inhomogeneity and the frequency-dependent dielectric constant of $SrTiO_3$:La,Rh photoelectrodes. The proposed phenomenological fitting accurately characterizes the system in Figure 6c, exhibiting a coefficient of determination near 0.99. Across all three samples, α values around 0.83 (Table S6) suggest a Cole−Cole relaxation model, where a dispersion of relaxation time constants is considered around the value of τ_n.[50,51] This model indicates deviations from an ideal Debye relaxation ($\alpha = 1$), which would present a perfect semicircle in the Nyquist plot. The V_{SS} parameter serves as an indicator of recombination degree in an illuminated semiconductor.[52]

For pristine $SrTiO_3$:La,Rh, $SrTiO_3$:La,Rh|H_2ase, and $SrTiO_3$:La,Rh|FDH, V_{SS} values were found to be 1.23 ± 0.01, 2.00 ± 0.01, and 1.73 ± 0.01 mV, respectively. This indicates that both enzymes contributed to a decrease in charge recombination. Moreover, the introduction of H_2ase and FDH onto $SrTiO_3$:La,Rh reduced τ_n from 466 ± 7.0 μs to 379 ± 12.0 and 412 ± 10.0 μs, respectively. This reduction can be attributed to the efficient extraction of photogenerated charges to enzymes upon irradiation, facilitating catalytic reactions and thus decreasing τ_n.

Attempts to study the charge transfer rate constant with intensity-modulated photocurrent spectroscopy (IMPS) were unsuccessful due to a low signal-to-noise ratio, which prevented the construction of a Nyquist plot. This issue is likely a result of the low photocurrent response (a few μA) of photoelectrodes made with $SrTiO_3$:La,Rh nanoparticles. Given a 10% incident light modulation depth, a minimum photocurrent response of approximately 100 μA is required to generate meaningful Nyquist plots. Although $SrTiO_3$ is an effective light absorber for photocatalysis, the morphology significantly impacts photocurrent generation. Unlike high-performing metal oxide photoelectrodes (*e.g.*, hematite and Cu_2O) fabricated through hydrothermal growth or electrodeposition to achieve large crystal grain sizes, our $SrTiO_3$:La,Rh photoelectrodes maintain a morphology of poorly connected nanoparticles, resulting in numerous interfaces that act as charge recombination centers.

CONCLUSIONS

This work establishes semiartificial colloidal Z-scheme photosynthesis for the selective synthesis of solar fuels without the requirement for sacrificial reagents. The semiartificial colloidal photosynthetic Z-scheme is versatile, easy to assemble and achieved effective H_2 production or CO_2 reduction using water as the electron donor. The developed H_2ase|$SrTiO_3$:La,Rh|$[Co(bpy)_3]^{3+/2+}$|$BiVO_4$:Mo|RuO_2 system yielded 506 ± 36

https://doi.org/10.1021/jacs.4c11827
J. Am. Chem. Soc. 2024, 146, 29865−29876

μmol H_2 g^{-1} with a TON of 50,550 and FDH|$SrTiO_3$:La,Rh|$[Co(bpy)_3]^{3+/2+}$|$BiVO_4$:Mo|RuO_2 yielded 319 ± 27 μmol formate g^{-1} with a TON of 12,740. Mott−Schottky analysis and cyclic voltammetry confirmed an energy band alignment suitable for a Z-scheme system between $SrTiO_3$:La,Rh and $BiVO_4$:Mo, along with determining the formal potential of the $[Co(bpy)_3]^{3+/2+}$ electron mediator within their respective band gaps. QCM analysis provided insights into the rapid adsorption process and strong binding interactions of H_2ase and FDH onto the $SrTiO_3$:La,Rh surface. Furthermore, a comprehensive suite of photoelectrochemical techniques (PEIS, TPC, and IMVS) were employed to investigate charge carrier dynamics, encompassing charge transfer, transport, and recombination processes. PEIS revealed significant reductions of R_{ct} (57% for H_2ase and 45% for FDH) and enhanced k_{ct} (192% for H_2ase and 84% for FDH) compared to pristine $SrTiO_3$:La,Rh, indicating improved charge transfer efficiency upon enzyme integration. TPC demonstrated that both enzymes facilitate the charge transport process, evidenced by a decreased τ_t upon interfacing $SrTiO_3$:La,Rh with enzymes. IMVS analysis showed 19% and 12% reductions of τ_n upon introducing H_2ase and FDH, respectively, reflecting efficient extraction of photogenerated electrons to enzymes under irradiation.

EXPERIMENTAL SECTION

Materials. The following chemicals and materials were purchased from commercial suppliers and used without further purification: N_2 and CO_2 gas bottles (2% CH_4 as internal standard, BOC), carbon-^{13}C dioxide ($^{13}CO_2$, Sigma-Aldrich, 99.0 atom % ^{13}C), O_2 cylinder industrial grade (99.5%, BOC), strontium carbonate ($SrCO_3$, Alfa Aesar, 99.99%), rutile titanium dioxide (TiO_2, Sigma-Aldrich, ≥99.98%), lanthanum oxide (La_2O_3, Fisher Scientific, 99.99%), rhodium(III) oxide (Rh_2O_3, Wako Pure Chemical, 98.0−102.0%), molybdenum trioxide (MoO_3, BDH Chemicals, 99.5%), vanadium(V) oxide (V_2O_5, Fisher Scientific, 99.6%), bismuth(III) nitrate pentahydrate ($Bi(NO_3)_3{\cdot}5H_2O$, Sigma-Aldrich, 98%), ruthenium(III) chloride hydrate ($RuCl_3{\cdot}xH_2O$, Acros Organics, 35−40% Ru), cobalt(II) sulfate heptahydrate ($CoSO_4{\cdot}7H_2O$, Acros Organics, 99+ %), 2,2′-bipyridine ($C_{10}H_8N_2$, Alfa Aesar, 98%), DL-dithiothreitol (DTT, Sigma-Aldrich, >99.5%), 2-amino-2-(hydroxymethyl)-1,3-propanediol (Tris base, Sigma-Aldrich, ≥99.8%), hydrochloric acid (HCl, Honeywell Fluka, 37%), sodium bicarbonate ($NaHCO_3$, Sigma-Aldrich, ≥99.9%), sodium bicarbonate-^{13}C ($NaH^{13}CO_3$, Sigma-Aldrich, 98 atom % ^{13}C), sodium formate (HCOONa, Sigma-Aldrich, ≥ 99.0%), sodium formate-^{13}C ($H^{13}COONa$, Sigma-Aldrich, 99 atom % ^{13}C), isopropanol ($(CH_3)_2CHOH$, Sigma-Aldrich, ≥99.5%), methanol (CH_3OH, anhydrous, Sigma-Aldrich, 99.8%), ethanol (C_2H_5OH, Sigma-Aldrich, 96%), deuterium oxide (D_2O, Sigma-Aldrich, 99.9 atom % D, contains 0.75 wt % 3-(trimethylsilyl)propionic-2,2,3,3-d_4 acid, sodium salt), Nafion perfluorinated resin solution (Sigma-Aldrich, 5 wt % in mixture of lower aliphatic alcohols and water, contains 45% water), Toray carbon paper (TGP-H-60, Thermo Scientific Chemicals), fluorine doped tin oxide (FTO) coated glass slide (2 cm × 10 cm, Pilkington TEC 15, Xop Glass, 12−14 Ω/sq), Parafilm (Bemis), and rubber septa (Subaseal). Milli-Q H_2O (18.2 MΩ cm) was used for all of the experiments. [W]-FDH and [NiFeSe]-H_2ase from *D. vulgaris* Hildenborough (*Dv*H) were expressed and purified according to previously reported methods.[23,24]

Synthesis of La,Rh Codoped $SrTiO_3$. La,Rh codoped strontium titanate, denoted as $SrTiO_3$:La,Rh, was synthesized by a two-step, solid-state reaction based on a previously reported procedure.[12,13] $SrCO_3$ was preheated at 573 K in air for 1 h before mixing with TiO_2 in a mortar at a Sr/Ti molar ratio of 1.05. The mixture was heated to 1473 K (10 K min^{-1}) for 10 h in an alumina crucible. The resulting $SrTiO_3$ was cooled down naturally to room temperature before mixing with La_2O_3 at a La/(La + Sr) ratio of 4 mol % and Rh_2O_3 at a Rh/(Rh + Ti) ratio of 4 mol %. The mixture was heated to 1373 K for 6 h to obtain $SrTiO_3$:La,Rh with La/(La + Sr)═Rh/(Rh + Ti) = 4 mol %.

Synthesis of RuO_2-Loaded Mo-Doped $BiVO_4$. Mo-doped bismuth vanadate, denoted as $BiVO_4$:Mo (Mo/V = 0.05 mol %), was prepared following literature.[53] K_2CO_3, MoO_3, and V_2O_5 (molar ratio of 1.05:0.05:1) were calcined in air at 723 K for 5 h to form a layered Mo-doped $K_3V_5O_{14}$ precursor. A suspension of $BiONO_3$ was prepared by adding stoichiometric $Bi(NO_3)_3{\cdot}5H_2O$ to distilled water. The Mo-doped $K_3V_5O_{14}$ was added to this suspension, and the mixture was stirred at 343 K for 10 h. The resulting $BiVO_4$:Mo was collected by filtration and washed with distilled water. RuO_2 cocatalyst (1 wt %) was deposited onto $BiVO_4$:Mo *via* impregnation.[13] 100 mg of $BiVO_4$:Mo and 751.3 μL of 0.01 M $RuCl_3$ solution were added to an evaporating dish. The mixture was briefly sonicated to disperse the $BiVO_4$:Mo. The mixture was stirred continuously while being evaporated over a water bath. The obtained powder was calcined in air at 623 K for 1 h.

Synthesis of $[Co(bpy)_3]SO_4$. Degassed water (15 mL) was added under vacuum to a Schlenk tube containing 2,2′-bipyridine (bpy, 258 mg, 1.65 mmol) and $Co(SO_4){\cdot}7H_2O$ (139 mg, 0.49 mmol) and the suspension was stirred under N_2 for 10 min.[14,34] Subsequently, dry methanol (15 mL) was added under low pressure and continuous stirring. The Schlenk tube was then evacuated and purged with N_2 for 15 min before the orange-yellow solution was heated to 90 °C for 2 h. After cooling down the reaction, it was taken to dryness and the mustard-colored solid was suspended in chloroform (20 mL), briefly sonicated and filtered off. The resulting mustard-colored solid was washed with chloroform (2 mL × 15 mL) and diethyl ether (2 mL × 15 mL) and dried under vacuum overnight to yield a mustard crystalline powder (300 mg, 81%, Figure S15). The reaction scheme is shown in Figure S14. Elemental analysis; calc. for $C_{30}H_{24}N_6O_4SCo{\cdot}7.05H_2O$ (M = 750.56 g mol^{-1}): C: 48.01, H 5.12, N 11.20%. Found: C 48.07, H 4.65, N 10.73%. ^{1}H NMR (D_2O, 400 MHz): δ (ppm) = 87.99 (bs, 6H_a), 83.46 (s, 6H_d), 45.91 (s, 6H_c), 14.52 (s, 6H_b). ESI-MS (+, water): m/z calc. for $C_{30}H_{24}N_6Co^{2+}$ (*i.e.*, M^{2+}): 263.5692, found: 263.5704; calc. for $C_{30}H_{24}N_6Co^{+}$ (*i.e.*, M^{+}): 527.1383, found: 527.1507; calc. for $C_{30}H_{25}N_6Co^{+}$ (*i.e.*, $[M + H^+]^+$): 528.1462, found: 528.1493. UV−vis (50 mM KCl, 100 mM $NaHCO_3$ in H_2O): λ_{max} (nm) (ε, M^{-1} cm^{-1}) = 435 (101). ATR-FTIR: v (cm^{-1}) = 3229, 3076, 1672, 1597, 1470, 1440, 1312, 1055, 1019, 775, 737.

Physical Characterizations. SEM images were acquired on a TESCAN MIRA3 field emission-gun-scanning electron microscope (FEG-SEM). TEM images were acquired on a Thermo Scientific (FEI) Talos F200X G2 TEM. EDX spectroscopy was carried out on the TESCAN MIRA3 FEG-SEM equipped with an Oxford Instruments Aztec Energy X-Max^N 80 mm^2 silicon drift detector. XPS data were acquired on a Thermo Scientific Escalab 250Xi fitted with a monochromated aluminum Kα X-ray source (1486.7 eV) at a pressure below 10−8 Torr and a room temperature of 294 K. XRD patterns were measured with a Malvern Panalytical Empyrean Series 2 X-ray diffractometer using Cu Kα irradiation operated at a 40 kV generator voltage and 40 mA tube current. Elemental analysis was carried out by using a PerkinElmer 240 elemental analyzer. High-resolution mass spectra were recorded on an Agilent 1260 Infinity LC system coupled to an Agilent 6230 time-of-flight liquid chromatography−mass spectrometry (LC/MS) system. ^{1}H NMR spectra were collected with a 500 MHz Avance III Smart Probe NMR spectrometer at room temperature. Chemical shifts for ^{1}H NMR spectra are referenced relative to residual protons in the deuterated solvent (Eurisotop), and 3-(trimethylsilyl)propionic-2,2,3,3-d_4 acid, sodium salt, in D_2O was used as the internal standard (TSP). ATR-FTIR spectra were recorded on a Nicolet iS50 spectrometer. UV−vis spectra were collected using a Cary 60 UV−vis spectrometer.

Photocatalysis. Photoreactor information and lamp setup can be found in Figures S24 and S25. For Z-scheme half reactions, either $SrTiO_3$:La,Rh (1 mg) or $BiVO_4$:Mo|RuO_2 (1 mg) was ultrasonicated for 30 min and dispersed in an aqueous solution (1 mL) containing $NaHCO_3$ (0.1 M) and $[Co(bpy)_3]^{3+/2+}$ (0.5 mM). For $SrTiO_3$:La,Rh experiments, either H_2ase (20 pmol) or FDH (50 pmol) was added

https://doi.org/10.1021/jacs.4c11827
J. Am. Chem. Soc. 2024, 146, 29865−29876

anaerobically. For Z-scheme reactions, $SrTiO_3$:La,Rh (1 mg) was ultrasonicated for 30 min and dispersed in an aqueous solution (0.5 mL) containing $NaHCO_3$ (0.1 M) and $[Co(bpy)_3]SO_4$ (0.5 mM). The $SrTiO_3$:La,Rh suspension was first anaerobically mixed with either H_2ase (20 pmol) or FDH (50 pmol) in the dark for 30 min, then mixed with $BiVO_4$:Mo|RuO_2 (1 mg in 0.5 mL) suspension containing $NaHCO_3$ (0.1 M) and $[Co(bpy)_3]SO_4$ (0.5 mM). All of the photoreactors were assembled in an anaerobic glovebox (MBraun, N_2 atmosphere, <0.1 ppm of O_2) and purged with CO_2 for 10 min. During photocatalysis, the photoreactors were illuminated under simulated AM 1.5G (100 mW cm^{-2}, Newport xenon arc lamp housing 66,921) and stirred at 600 rpm at 25 °C. For visible light-driven photocatalysis, a 420 nm long-pass filter was positioned in front of the photoreactors. Prior semiconductor−enzyme assembly, FDH was incubated with DTT solution (80 mM) in Tris-HCl buffer (20 mM, pH 9) for 10 min to activate the enzymes.[24]

Product Quantification. The amount of H_2 produced was analyzed by headspace gas analysis using a Shimadzu Tracera GC-2010 Plus with a barrier discharge ionization detector. The GC-2010 Plus was equipped with a ShinCarbon micro ST column (0.53 mm diameter) kept at 40 °C using helium carrier gas. Aliquots of the headspace gas (100 μL) were removed from the sealed photocatalytic reactors using a gastight syringe (Hamilton) for GC analysis. CH_4 was used as an internal standard. The amount of formate produced was quantified by ion chromatography (IC) using a Metrohm 882 Compact IC Plus ion chromatograph with a conductivity detector and a pump pressure of around 10 MPa. The eluent buffer contained Na_2CO_3 (3 mM) and $NaHCO_3$ (1 mM) in H_2O. Aliquots of the photocatalysis solution were removed from the sealed photocatalytic reactors and diluted 10 times with H_2O before injecting into the ion chromatograph *via* a 220 nm syringe filter. O_2 was quantified by a NeoFox-GT fluorometer and Fospor-R fluorescence oxygen sensor probe (Ocean Optics) in a glovebox (Belle Technology, N_2 atmosphere, <1 ppm of O_2).

Determination of $[Co(bpy)_3]^{3+/2+}$ Concentrations. The quantification method is based on the work of Mulazzani et al.[36] and Kudo et al.[14] using the Beer−Lambert law: $A = \varepsilon cl$, where A is the absorbance, ε is the molar absorption coefficient (M^{-1} cm^{-1}), c is the molar concentration (M), and l is the optical path length (cm).

Isotopic Labeling. Photocatalysis experiments were carried out in either a $NaH^{12}CO_3$ (0.1 M) aqueous solution with $^{12}CO_2$ as the headspace gas or a $NaH^{13}CO_3$ (0.1 M) aqueous solution with $^{13}CO_2$ as the headspace gas. After 10 h of simulated AM 1.5G irradiation, the solution was transferred to an NMR tube, and ^{1}H NMR spectra were collected with a 400 MHz NMR spectrometer. ^{1}H NMR spectra of commercial sodium formate-^{12}C ($H^{12}COONa$) and sodium formate-^{13}C ($H^{13}COONa$) were recorded to compare with the ^{1}H NMR spectra of the labeled products (Figure S22).

Apparent Quantum Yield (AQY). AQY measurements were conducted on a solar simulator (LOT-Quantum Design , LSN254) with a monochromator (LOT-Quantum Design, MSH300) at a 420 nm wavelength. The incident light was measured by a power meter (Thorlabs, PM100D) with a thermal power sensor (Thorlabs, S302C). The calculation of AQY for the Z-scheme reactions is based on the two-step photoexcitation mechanism: the production of one H_2 or formate molecule requires the generation of two photoexcited electrons by $SrTiO_3$:La,Rh, and another two photoexcited electrons by $BiVO_4$:Mo|RuO_2 to recombine with the two holes in $SrTiO_3$:La,Rh *via* the redox mediator. Therefore, one produced H_2 or formate molecule requires four photoexcited electrons. The AQY is calculated by

$$\mathrm{AQY}(H_2) = \frac{4 \times n(H_2)}{n(\mathrm{photons})} \times 100\%$$

$$\mathrm{AQY}(HCOO^-) = \frac{4 \times n(HCOO^-)}{n(\mathrm{photons})} \times 100\%$$

where, $n(H_2)$, $n(HCOO^-)$, and n(photons) represent the number of produced H_2, number of produced formate, and number of incident photons, respectively.

Solar Energy Conversion Efficiency. The solar-to-H_2 energy conversion efficiency (STH) is described as

$$\mathrm{STH} = \frac{R(H_2) \times \Delta G_r}{P \times S} \times 100\%$$

where, $R(H_2)$, ΔG_r, P, and S are the rate of H_2 evolution, the reaction Gibbs energy of the water splitting (237.2 kJ mol^{-1}), the AM 1.5G irradiance (100 mW cm^{-2}), and the irradiated sample area (1 cm^2), respectively.

Similarly, the solar-to-formate energy conversion efficiency (STF) is given by

$$\mathrm{STF} = \frac{R(HCOO^-) \times \Delta G_r}{P \times S} \times 100\%$$

where, $R(HCOO^-)$ and ΔG_r are the rate of formate evolution and the reaction Gibbs energy of the CO_2-to-formate conversion (238 kJ mol^{-1}), respectively.

Quartz Crystal Microbalance (QCM). QCM experiments were performed using a Biolin Q-Sense Explorer module and a custom-designed QCM cell within an anaerobic glovebox (MBraun, N_2 atmosphere, <0.1 ppm of O_2). A gold-coated quartz chip with a surface area of 0.79 cm^2 and a surface roughness <1 nm RMS was utilized. The chip was initially functionalized by drop-casting an ultrasonicated suspension (0.1 mL) of $SrTiO_3$:La,Rh (0.5 mg mL^{-1}) in isopropyl alcohol, forming a thin layer on the surface. To establish a stable baseline, prior to measurements, an enzyme-free aqueous solution (2 mL) containing $NaHCO_3$ (0.1 M) and $[Co(bpy)_3]SO_4$ (0.5 mM) was flowed through the system at a rate of 0.141 mL min^{-1} for a duration of at least 1 h. Once the baseline reached a steady state, 50 pmol of enzyme (either H_2ase or FDH) was introduced into the buffer solution (2 mL) for evaluating enzyme loading for 2 h. Subsequently after enzyme loading, a washing process was performed by flowing an enzyme-free aqueous solution (10 mL) containing $NaHCO_3$ (0.1 M) and $[Co(bpy)_3]SO_4$ (0.5 mM) at a rate of 0.141 mL min^{-1} for a duration of 1 h. The adsorption and desorption of the enzyme onto the surface was quantified by monitoring changes in the resonance frequency of the piezoelectric quartz chip. To determine the corresponding mass change, the change in frequency (Δf) was analyzed using the Sauerbrey equation:[41]

$$\Delta f = -\frac{2f_0^2}{A\sqrt{p_q \mu_q}} \Delta m$$

where, f_0 is the resonance frequency (5 MHz) of the quartz oscillator, A is the piezoelectrically active crystal area, Δm is the change in mass, p_q is the density of quartz, and μ_q is the shear modulus of quartz. Assuming 25% of the adsorbed mass consisted of water molecules bound to the enzymes, Δm can be converted into the quantity of enzymes.

Electrode Fabrication. The thin-film electrodes were made by depositing nanoparticle suspension in isopropanol on a FTO-coated glass, adapting a literature procedure.[12,13] A 0.25 cm^2 Parafilm template, made with a drilling bill, was pressed onto the FTO side (1 cm × 2 cm) and slightly heated (10 s in a 150 °C drying oven) to ensure uniform adhesion of the mask to the slide. The suspensions of $SrTiO_3$:La,Rh, $BiVO_4$:Mo, or $BiVO_4$:Mo|RuO_2 were dispersed in isopropanol at a concentration of 10 mg mL^{-1} and ultrasonicated for 2 min. In total, 50 μL of the suspension was drop-cast onto the masked FTO glass in 4 equal layers (12.5 μL per layer) and allowed to dry in air. For $SrTiO_3$:La,Rh and $BiVO_4$:Mo|RuO_2 electrodes, the mask was removed and the samples were annealed for 1 h at 573 K in air (ramp rate 5 °C min^{-1}). For $BiVO_4$:Mo electrodes, 2 μL of Nafion solution was diluted in 50 μL of isopropanol then drop-cast onto $BiVO_4$:Mo and allowed to dry in air. Photographs of these thin-film electrodes demonstrate that the metal oxide semiconductors have been homogeneously deposited onto a well-defined area (0.25 cm^2),

https://doi.org/10.1021/jacs.4c11827
J. Am. Chem. Soc. 2024, 146, 29865−29876

ensuring high quality and uniformity of the thin-film electrodes (Figure S26).

Electrochemical Impedance Spectroscopy (EIS). EIS experiments were performed in an electrochemical cell with a three-electrode configuration: a working electrode (either $SrTiO_3$:La,Rh or $BiVO_4$:Mo), a Pt mesh counter electrode, and a RE-6 Ag/AgCl reference electrode (3 M NaCl gel, 0.55 mm diameter ceramic frit, MW-2030, BASi). 50 pmol of enzymes (either H_2ase or FDH) was drop-cast onto the working electrode. The anaerobic electrolyte (20 mL) contains CO_2-saturated $NaHCO_3$ (0.1 M), pH 6.7, KCl (50 mM), and $[Co(bpy)_3]SO_4$ (0.5 mM). Photoelectrochemical impedance spectroscopy (PEIS) measurements were carried out under AM 1.5G irradiation where a 150 W xenon arc lamp (LOT-Quantum Design , LSE140/160.25C) was used as a light source. Impedance response was recorded at −0.2 V *vs* RHE with a potentiostat (IviumStat) with frequency ranges from 100 kHz to 50 mHz and a 25 mV sinusoidal amplitude. Impedance data was fitted with equivalent circuits using modeling software ZView2 (Scribner Associates).

Transient Photocurrent Spectroscopy (TPC). TPC measurements were conducted in a single compartment electrochemical cell with a three-electrode configuration containing a $SrTiO_3$:La,Rh working electrode, a Pt mesh counter electrode, and a RE-6 Ag/AgCl reference electrode (3 M NaCl gel, 0.55 mm diameter ceramic frit, MW-2030, BASi). 50 pmol of enzymes (either H_2ase or FDH) were drop-cast onto the working electrode. The anaerobic electrolyte (20 mL) contains CO_2-saturated $NaHCO_3$ (0.1 M), pH 6.7, KCl (50 mM), and $[Co(bpy)_3]SO_4$ (0.5 mM). An AM 1.5G solar light simulator (LOT-Quantum Design, LS0816-H/LSN558) with a built-in shutter was used as the light source. TPC response was recorded at −0.2 V *vs* RHE on a Bio-Logic VSP potentiostat. TPC data were normalized and fitted with exponential decay function using OriginPro 2021b (OriginLab).

Intensity-Modulated Photovoltage Spectroscopy (IMVS). IMVS measurements were carried out under open circuit conditions in a single compartment electrochemical cell with a two-electrode configuration containing a $SrTiO_3$:La,Rh working electrode and a RE-6 Ag/AgCl reference electrode (3 M NaCl gel, 0.55 mm diameter ceramic frit, MW-2030, BASi). 50 pmol of enzymes (either H_2ase or FDH) were drop-cast onto the working electrode. The anaerobic electrolyte (20 mL) contains CO_2-saturated $NaHCO_3$ (0.1 M), pH 6.7, KCl (50 mM), and $[Co(bpy)_3]SO_4$ (0.5 mM). A 470 nm blue LED (TruOpto, OSUB5111P, 5 mm, 12000 mcd) was used as the light source and was sinusoidally modulated (0.5 MHz to 0.5 Hz, ∼10% modulation depth) by a Bio-Logic VSP potentiostat. The open circuit voltage (V_{OC}) was recorded on a Bio-Logic VSP potentiostat.

■ ASSOCIATED CONTENT

Data Availability Statement

Data supporting the findings of this study are available from the University of Cambridge data repository: https://doi.org/10.17863/CAM.112500.

Supporting Information

The Supporting Information is available free of charge at https://pubs.acs.org/doi/10.1021/jacs.4c11827.

Tauc plots; Mott−Schottky plots; SEM images; TEM images; EDX mapping; XRD patterns; UV−vis spectra; ^{1}H NMR spectra; ATR-FTIR spectrum; photoreactor information; lamp setup; photograph of electrodes (PDF)

■ AUTHOR INFORMATION

Corresponding Author

Erwin Reisner − *Yusuf Hamied Department of Chemistry, University of Cambridge, Cambridge CB2 1EW, U.K.;* orcid.org/0000-0002-7781-1616; Email: reisner@ch.cam.ac.uk

Authors

Yongpeng Liu − *Yusuf Hamied Department of Chemistry, University of Cambridge, Cambridge CB2 1EW, U.K.;* orcid.org/0000-0002-4544-4217

Ariffin Bin Mohamad Annuar − *Yusuf Hamied Department of Chemistry, University of Cambridge, Cambridge CB2 1EW, U.K.*

Santiago Rodríguez-Jiménez − *Yusuf Hamied Department of Chemistry, University of Cambridge, Cambridge CB2 1EW, U.K.;* orcid.org/0000-0002-2979-8525

Celine Wing See Yeung − *Yusuf Hamied Department of Chemistry, University of Cambridge, Cambridge CB2 1EW, U.K.*

Qian Wang − *Yusuf Hamied Department of Chemistry, University of Cambridge, Cambridge CB2 1EW, U.K.;* Present Address: Graduate School of Engineering, Nagoya University, Furo-cho, Chikusa-ku, Nagoya 464−8603, Japan; orcid.org/0000-0002-8980-4915

Ana M. Coito − *Instituto de Tecnologia Química e Biológica António Xavier (ITQB NOVA), Universidade NOVA de Lisboa, 2780-157 Oeiras, Portugal*

Rita R. Manuel − *Instituto de Tecnologia Química e Biológica António Xavier (ITQB NOVA), Universidade NOVA de Lisboa, 2780-157 Oeiras, Portugal;* orcid.org/0000-0001-8068-2053

Inês A. C. Pereira − *Instituto de Tecnologia Química e Biológica António Xavier (ITQB NOVA), Universidade NOVA de Lisboa, 2780-157 Oeiras, Portugal;* orcid.org/0000-0003-3283-4520

Complete contact information is available at: https://pubs.acs.org/10.1021/jacs.4c11827

Author Contributions

‖Y.L. and A.B.M.A contributed equally to this work.

Notes

The authors declare no competing financial interest.

■ ACKNOWLEDGMENTS

We are grateful for support by the Swiss National Science Foundation (SNSF) for a Postdoc.Mobility fellowship (grant number P500PN_202908 to Y.L), the Leverhulme Early Career Fellowship (ECF-2024-230 to Y.L.), an Isaac Newton Trust (INT) Early Career Fellowship (23.23(g) and 24.08(s) to Y.L.), the Petronas Education Sponsorship Program for Postgraduate Studies (to A.B.M.A.), the European commission for a Horizon 2020 Marie Sklodowska-Curie individual Fellowship (GAN 891338 to S.R.J.), the Singapore Agency for Science, Technology, and Research (A*STAR) for a Ph.D. studentship (to C.W.S.Y.), the European Research Council (ERC) for a Consolidator Grant (MatEnSAP, 682833 to E.R.) and a UKRI/ERC Advanced Grant (EP/X030563/1 to E.R.). We also acknowledge support from the Fundação para a Ciência e Tecnologia (FCT) for PTDC/BII-BBF/2050/2020 grant and MOSTMICRO-ITQB unit (UIDB/04612/2020 and UIDP/04612/2020), and LS4FUTURE Associated Laboratory (LA/P/0087/2020 to I.A.C.P.), the FCT for PhD fellowship DFA/BD/7897/2020 (to R.R.M.) and SFRH/BD/146475/2019 (to A.M.C.). We thank Dr. Leonardo Castañeda-Losada and Mr. Dongseok Kim for helpful discussions.

REFERENCES

(1) Xue, J.; Fujitsuka, M.; Tachikawa, T.; Bao, J.; Majima, T. Charge Trapping in Semiconductor Photocatalysts: A Time- and Space-Domain Perspective. *J. Am. Chem. Soc.* **2024**, *146* (13), 8787−8799.

(2) Wang, Q.; Pornrungroj, C.; Linley, S.; Reisner, E. Strategies to Improve Light Utilization in Solar Fuel Synthesis. *Nat. Energy* **2022**, *7* (1), 13−24.

(3) Nocera, D. G. Proton-Coupled Electron Transfer: The Engine of Energy Conversion and Storage. *J. Am. Chem. Soc.* **2022**, *144* (3), 1069−1081.

(4) Meng, S.-L.; Ye, C.; Li, X.-B.; Tung, C.-H.; Wu, L.-Z. Photochemistry Journey to Multielectron and Multiproton Chemical Transformation. *J. Am. Chem. Soc.* **2022**, *144* (36), 16219−16231.

(5) Yoshino, S.; Takayama, T.; Yamaguchi, Y.; Iwase, A.; Kudo, A. CO_2 Reduction Using Water as an Electron Donor over Heterogeneous Photocatalysts Aiming at Artificial Photosynthesis. *Acc. Chem. Res.* **2022**, *55* (7), 966−977.

(6) Bard, A. J. Photoelectrochemistry and Heterogeneous Photo-Catalysis at Semiconductors. *J. Photochem.* **1979**, *10* (1), 59−75.

(7) Abe, R.; Sayama, K.; Domen, K.; Arakawa, H. A New Type of Water Splitting System Composed of Two Different TiO_2 Photocatalysts (Anatase, Rutile) and a IO_3^-/I^- Shuttle Redox Mediator. *Chem. Phys. Lett.* **2001**, *344* (3), 339−344.

(8) Iwashina, K.; Iwase, A.; Ng, Y. H.; Amal, R.; Kudo, A. Z-Schematic Water Splitting into H_2 and O_2 Using Metal Sulfide as a Hydrogen-Evolving Photocatalyst and Reduced Graphene Oxide as a Solid-State Electron Mediator. *J. Am. Chem. Soc.* **2015**, *137* (2), 604−607.

(9) Wang, Q.; Hisatomi, T.; Ma, S. S. K.; Li, Y.; Domen, K. Core/Shell Structured La- and Rh-Codoped $SrTiO_3$ as a Hydrogen Evolution Photocatalyst in Z-Scheme Overall Water Splitting under Visible Light Irradiation. *Chem. Mater.* **2014**, *26* (14), 4144−4150.

(10) Takata, T.; Jiang, J.; Sakata, Y.; Nakabayashi, M.; Shibata, N.; Nandal, V.; Seki, K.; Hisatomi, T.; Domen, K. Photocatalytic Water Splitting with a Quantum Efficiency of Almost Unity. *Nature* **2020**, *581* (7809), 411−414.

(11) Konta, R.; Ishii, T.; Kato, H.; Kudo, A. Photocatalytic Activities of Noble Metal Ion Doped $SrTiO_3$ under Visible Light Irradiation. *J. Phys. Chem. B* **2004**, *108* (26), 8992−8995.

(12) Wang, Q.; Warnan, J.; Rodríguez-Jiménez, S.; Leung, J. J.; Kalathil, S.; Andrei, V.; Domen, K.; Reisner, E. Molecularly Engineered Photocatalyst Sheet for Scalable Solar Formate Production from Carbon Dioxide and Water. *Nat. Energy* **2020**, *5* (9), 703−710.

(13) Wang, Q.; Kalathil, S.; Pornrungroj, C.; Sahm, C. D.; Reisner, E. Bacteria−Photocatalyst Sheet for Sustainable Carbon Dioxide Utilization. *Nat. Catal.* **2022**, *5* (7), 633−641.

(14) Sasaki, Y.; Kato, H.; Kudo, A. $[Co(Bpy)_3]^{3+/2+}$ and $[Co(Phen)_3]^{3+/2+}$ Electron Mediators for Overall Water Splitting under Sunlight Irradiation Using Z-Scheme Photocatalyst System. *J. Am. Chem. Soc.* **2013**, *135* (14), 5441−5449.

(15) Qi, Y.; Zhang, J.; Kong, Y.; Zhao, Y.; Chen, S.; Li, D.; Liu, W.; Chen, Y.; Xie, T.; Cui, J.; Li, C.; Domen, K.; Zhang, F. Unraveling of Cocatalysts Photodeposited Selectively on Facets of $BiVO_4$ to Boost Solar Water Splitting. *Nat. Commun.* **2022**, *13* (1), No. 484.

(16) Park, H. S.; Kweon, K. E.; Ye, H.; Paek, E.; Hwang, G. S.; Bard, A. J. Factors in the Metal Doping of $BiVO_4$ for Improved Photoelectrocatalytic Activity as Studied by Scanning Electrochemical Microscopy and First-Principles Density-Functional Calculation. *J. Phys. Chem. C* **2011**, *115* (36), 17870−17879.

(17) Zhang, J. Z.; Reisner, E. Advancing Photosystem II Photoelectrochemistry for Semi-Artificial Photosynthesis. *Nat. Rev. Chem.* **2020**, *4* (1), 6−21.

(18) Martin, D. J.; Reardon, P. J. T.; Moniz, S. J. A.; Tang, J. Visible Light-Driven Pure Water Splitting by a Nature-Inspired Organic Semiconductor-Based System. *J. Am. Chem. Soc.* **2014**, *136* (36), 12568−12571.

(19) Tada, H.; Mitsui, T.; Kiyonaga, T.; Akita, T.; Tanaka, K. All-Solid-State Z-Scheme in CdS−Au−TiO_2 Three-Component Nanojunction System. *Nat. Mater.* **2006**, *5* (10), 782−786.

(20) Yella, A.; Lee, H.-W.; Tsao, H. N.; Yi, C.; Chandiran, A. K.; Nazeeruddin, Md. K.; Diau, E. W.-G.; Yeh, C.-Y.; Zakeeruddin, S. M.; Grätzel, M. Porphyrin-Sensitized Solar Cells with Cobalt(II/III)−Based Redox Electrolyte Exceed 12% Efficiency. *Science* **2011**, *334* (6056), 629−634.

(21) Mathew, S.; Yella, A.; Gao, P.; Humphry-Baker, R.; Curchod, B. F. E.; Ashari-Astani, N.; Tavernelli, I.; Rothlisberger, U.; Nazeeruddin, M. K.; Grätzel, M. Dye-Sensitized Solar Cells with 13% Efficiency Achieved through the Molecular Engineering of Porphyrin Sensitizers. *Nat. Chem.* **2014**, *6* (3), 242−247.

(22) Yoshino, S.; Sato, K.; Yamaguchi, Y.; Iwase, A.; Kudo, A. Z-Schematic CO_2 Reduction to CO through Interparticle Electron Transfer between $SrTiO_3$:Rh of a Reducing Photocatalyst and $BiVO_4$ of a Water Oxidation Photocatalyst under Visible Light. *ACS Appl. Energy Mater.* **2020**, *3* (10), 10001−10007.

(23) Marques, M. C.; Tapia, C.; Gutiérrez-Sanz, O.; Ramos, A. R.; Keller, K. L.; Wall, J. D.; De Lacey, A. L.; Matias, P. M.; Pereira, I. A. C. The Direct Role of Selenocysteine in [NiFeSe] Hydrogenase Maturation and Catalysis. *Nat. Chem. Biol.* **2017**, *13* (5), 544−550.

(24) Oliveira, A. R.; Mota, C.; Vilela-Alves, G.; Manuel, R. R.; Pedrosa, N.; Fourmond, V.; Klymanska, K.; Léger, C.; Guigliarelli, B.; Romão, M. J.; Pereira, I. A. C. An Allosteric Redox Switch Involved in Oxygen Protection in a CO_2 Reductase. *Nat. Chem. Biol.* **2024**, *20* (1), 111−119.

(25) Reisner, E.; Powell, D. J.; Cavazza, C.; Fontecilla-Camps, J. C.; Armstrong, F. A. Visible Light-Driven H_2 Production by Hydrogenases Attached to Dye-Sensitized TiO_2 Nanoparticles. *J. Am. Chem. Soc.* **2009**, *131* (51), 18457−18466.

(26) Badiani, V. M.; Casadevall, C.; Miller, M.; Cobb, S. J.; Manuel, R. R.; Pereira, I. A. C.; Reisner, E. Engineering Electro- and Photocatalytic Carbon Materials for CO_2 Reduction by Formate Dehydrogenase. *J. Am. Chem. Soc.* **2022**, *144* (31), 14207−14216.

(27) Sokol, K. P.; Robinson, W. E.; Oliveira, A. R.; Warnan, J.; Nowaczyk, M. M.; Ruff, A.; Pereira, I. A. C.; Reisner, E. Photoreduction of CO_2 with a Formate Dehydrogenase Driven by Photosystem II Using a Semi-Artificial Z-Scheme Architecture. *J. Am. Chem. Soc.* **2018**, *140* (48), 16418−16422.

(28) Sokol, K. P.; Robinson, W. E.; Warnan, J.; Kornienko, N.; Nowaczyk, M. M.; Ruff, A.; Zhang, J. Z.; Reisner, E. Bias-Free Photoelectrochemical Water Splitting with Photosystem II on a Dye-Sensitized Photoanode Wired to Hydrogenase. *Nat. Energy* **2018**, *3* (11), 944−951.

(29) Moore, E. E.; Andrei, V.; Oliveira, A. R.; Coito, A. M.; Pereira, I. A. C.; Reisner, E. A Semi-Artificial Photoelectrochemical Tandem Leaf with a CO_2-to-Formate Efficiency Approaching 1%. *Angew. Chem., Int. Ed.* **2021**, *60* (50), 26303−26307.

(30) Liu, Y.; Webb, S.; Moreno-García, P.; Kulkarni, A.; Maroni, P.; Broekmann, P.; Milton, R. D. Facile Functionalization of Carbon Electrodes for Efficient Electroenzymatic Hydrogen Production. *JACS Au* **2023**, *3* (1), 124−130.

(31) Kato, H.; Sasaki, Y.; Shirakura, N.; Kudo, A. Synthesis of Highly Active Rhodium-Doped $SrTiO_3$ Powders in Z-Scheme Systems for Visible-Light-Driven Photocatalytic Overall Water Splitting. *J. Mater. Chem. A* **2013**, *1* (39), 12327.

(32) Wei, Y.; Wan, J.; Wang, J.; Zhang, X.; Yu, R.; Yang, N.; Wang, D. Hollow Multishelled Structured $SrTiO_3$ with La/Rh Co-Doping for Enhanced Photocatalytic Water Splitting under Visible Light. *Small* **2021**, *17* (22), No. 2005345.

(33) Parmar, K. P. S.; Kang, H. J.; Bist, A.; Dua, P.; Jang, J. S.; Lee, J. S. Photocatalytic and Photoelectrochemical Water Oxidation over Metal-Doped Monoclinic $BiVO_4$ Photoanodes. *ChemSusChem* **2012**, *5* (10), 1926−1934.

(34) Jaeger, F. M.; Dijk, J. A. Die Verschiedenen Typen von Komplexsalzen Des α-A′-Dipyridyls Mit Kupfer, Zink, Cadmium, Eisen, Nickel, Kobalt Und Rhodium. *Z. Anorg. Allg. Chem.* **1936**, *227* (3), 273−327.

https://doi.org/10.1021/jacs.4c11827
J. Am. Chem. Soc. 2024, 146, 29865−29876

(35) Liu, Y.; Pulignani, C.; Webb, S.; Cobb, S. J.; Rodríguez-Jiménez, S.; Kim, D.; Milton, R. D.; Reisner, E. Electrostatic [FeFe]-Hydrogenase−Carbon Nitride Assemblies for Efficient Solar Hydrogen Production. *Chem. Sci.* **2024**, *15* (16), 6088−6094.
(36) Simic, M. G.; Hoffman, M. Z.; Cheney, R. P.; Mulazzani, Q. G. One-Electron Reduction of Tris(2,2′-Bipyridine) and Tris(1,10-Phenanthroline) Complexes of Cobalt(III) in Aqueous Solution. *J. Phys. Chem. A* **1979**, *83* (4), 439−443.
(37) Yamasaki, K.; Hara, T.; Yasuda, M. Absorption Spectra of Cobalt Complexes with 1, 10-Phenanthroline. *Proc. Jpn. Acad.* **1953**, *29* (7), 337−341.
(38) Yamaguchi, K.; Kume, S.; Namiki, K.; Murata, M.; Tamai, N.; Nishihara, H. UV−Vis, NMR, and Time-Resolved Spectroscopy Analysis of Photoisomerization Behavior of Three- and Six-Azobenzene-Bound Tris(Bipyridine)Cobalt Complexes. *Inorg. Chem.* **2005**, *44* (24), 9056−9067.
(39) Iwashina, K.; Kudo, A. Rh-Doped $SrTiO_3$ Photocatalyst Electrode Showing Cathodic Photocurrent for Water Splitting under Visible-Light Irradiation. *J. Am. Chem. Soc.* **2011**, *133* (34), 13272−13275.
(40) Nishiyama, H.; Yamada, T.; Nakabayashi, M.; Maehara, Y.; Yamaguchi, M.; Kuromiya, Y.; Nagatsuma, Y.; Tokudome, H.; Akiyama, S.; Watanabe, T.; Narushima, R.; Okunaka, S.; Shibata, N.; Takata, T.; Hisatomi, T.; Domen, K. Photocatalytic Solar Hydrogen Production from Water on a 100-m^2 Scale. *Nature* **2021**, *598* (7880), 304−307.
(41) Sauerbrey, G. Verwendung von Schwingquarzen zur Wägung dünner Schichten und zur Mikrowägung. *Z. Phys.* **1959**, *155* (2), 206−222.
(42) Warburg, E. Ueber Die Spitzenentladung. *Ann. Phys.* **1899**, *303* (1), 69−83.
(43) Randles, J. E. B. Kinetics of Rapid Electrode Reactions. *Discuss. Faraday Soc.* **1947**, *1*, 11−19.
(44) Wieczorek, A.; Liu, Y.; Cho, H.-H.; Sivula, K. Assessing the Charge Carrier Dynamics at Hybrid Interfaces of Organic Photoanodes for Solar Fuels. *J. Phys. Chem. Lett.* **2024**, *15* (24), 6347−6354.
(45) Xu, P.; Gray, C. L.; Xiao, L.; Mallouk, T. E. Charge Recombination with Fractional Reaction Orders in Water-Splitting Dye-Sensitized Photoelectrochemical Cells. *J. Am. Chem. Soc.* **2018**, *140* (37), 11647−11654.
(46) Liu, Y.; Bouri, M.; Yao, L.; Xia, M.; Mensi, M.; Grätzel, M.; Sivula, K.; Aschauer, U.; Guijarro, N. Identifying Reactive Sites and Surface Traps in Chalcopyrite Photocathodes. *Angew. Chem., Int. Ed.* **2021**, *60* (44), 23651−23655.
(47) Liu, Y.; Quiñonero, J.; Yao, L.; Pereira, X. D. C.; Mensi, M.; Gómez, R.; Sivula, K.; Guijarro, N. Defect Engineered Nanostructured $LaFeO_3$ Photoanodes for Improved Activity in Solar Water Oxidation. *J. Mater. Chem. A* **2021**, *9* (5), 2888−2898.
(48) Boudoire, F.; Liu, Y.; Le Formal, F.; Guijarro, N.; Lhermitte, C. R.; Sivula, K. Spray Synthesis of $CuFeO_2$ Photocathodes and In-Operando Assessment of Charge Carrier Recombination. *J. Phys. Chem. C* **2021**, *125* (20), 10883−10890.
(49) Liu, Y.; Guijarro, N.; Sivula, K. Understanding Surface Recombination Processes Using Intensity-Modulated Photovoltage Spectroscopy on Hematite Photoanodes for Solar Water Splitting. *Helv. Chim. Acta* **2020**, *103* (6), No. e2000064.
(50) Cole, K. S.; Cole, R. H. Dispersion and Absorption in Dielectrics I. Alternating Current Characteristics. *J. Chem. Phys.* **1941**, *9* (4), 341−351.
(51) Liu, Y.; Xia, M.; Ren, D.; Nussbaum, S.; Yum, J.-H.; Grätzel, M.; Guijarro, N.; Sivula, K. Photoelectrochemical CO_2 Reduction at a Direct $CuInGaS_2$/Electrolyte Junction. *ACS Energy Lett.* **2023**, *8* (4), 1645−1651.
(52) O'Regan, B. C.; Lenzmann, F. Charge Transport and Recombination in a Nanoscale Interpenetrating Network of N-Type and p-Type Semiconductors: Transient Photocurrent and Photovoltage Studies of TiO_2/Dye/CuSCN Photovoltaic Cells. *J. Phys. Chem. B* **2004**, *108* (14), 4342−4350.
(53) Kudo, A.; Omori, K.; Kato, H. A Novel Aqueous Process for Preparation of Crystal Form-Controlled and Highly Crystalline $BiVO_4$ Powder from Layered Vanadates at Room Temperature and Its Photocatalytic and Photophysical Properties. *J. Am. Chem. Soc.* **1999**, *121* (49), 11459−11467.

https://doi.org/10.1021/jacs.4c11827
J. Am. Chem. Soc. 2024, 146, 29865−29876